Fermi National Accelerator Laboratory

FERMILAB-Conf-96/143-E
D0

Electroweak Measurements from the Tevatron

Ulrich Heintz
For the D0 and CDF Collaborations

Fermi National Accelerator Laboratory
P.O. Box 500, Batavia, Illinois 60510

June 1996

Presented at the *Les Rencontres de Physique de la Vallee d'Aoste,*
La Thuile, Italy, March 3-9, 1996

Operated by Universities Research Association Inc. under Contract No. DE-AC02-76CHO3000 with the United States Department of Energy

Disclaimer

FERMILAB CONF-96/143-E

ELECTROWEAK MEASUREMENTS FROM THE TEVATRON [1]

Ulrich Heintz

Fermi National Accelerator Laboratory
P. O. Box 500
Batavia, IL 60510

Abstract

The two detectors at the Fermilab Tevatron, DØ and CDF, have collected large samples of W and Z decays. With these data measurements of the properties of the W boson have been performed. From the ratio of the W and Z production cross sections a measurement of the W boson width of 2.062 ± 0.059 GeV has been obtained. The W boson mass has been measured to be 80.34 ± 0.15 GeV. Both detectors have observed diboson production and measured the triple gauge boson couplings. No deviations from Standard Model predictions have been observed.

[1] presented at Les Rencontres de Physique de la Vallée d'Aoste, La Thuile, Italy, March 3–9, 1996.

1 Introduction

The Fermilab Tevatron, which collides protons and antiprotons at a center of mass energy of $\sqrt{s} = 1.8$ TeV, is presently the only source of large samples of W boson decays. During Run 1 of the Tevatron, which lasted from 1992 to 1996 and proceeded in three phases, Run 1a (1992/93), Run 1b (1994/95) and Run 1c (1996), the Tevatron reached a peak luminosity of 2.5×10^{31} cm^{-2}s^{-1}. The DØ and CDF detectors both collected large data samples (see table 1). Here I report on the electroweak measurements performed using the data collected during Run 1a and 1b.

detector	Run 1a	Run 1b	Run 1c
DØ	15 pb^{-1}	89 pb^{-1}	13 pb^{-1}
CDF	20 pb^{-1}	90 pb^{-1}	7 pb^{-1}

Table 1: Integrated luminosities for DØ and CDF data sets.

2 W and Z boson production

In $p\overline{p}$ collisions W and Z bosons are produced at lowest order in $q\overline{q}$ annihilation. They are tagged by their leptonic decay modes. $W \to \ell\nu$ decays are characterized by a charged lepton ($e^{\pm}$, $\mu^{\pm}$) with high transverse momentum (p_T) and high missing transverse momentum ($\not{p}_T$) due to the unobserved neutrino. Since the component of the neutrino momentum along the beam direction is unknown we characterize the events by the transverse mass of the charged lepton and the neutrino,

$$m_T = \sqrt{2 p_T \not{p}_T (1 - cos\Delta\phi)}, \tag{1}$$

where $\Delta\phi$ is the azimuthal separation of the charged lepton and the neutrino.

Both experiments have measured the W and Z boson production cross sections times leptonic branching fraction (σB). Figure 1 shows the transverse mass spectrum of the DØ $W \to e\nu$ candidate sample and the invariant mass spectrum of the $Z \to ee$ candidate sample from Run 1b. Table 2 summarizes the cross section analyses with number of candidate events, estimated backgrounds, acceptance$\times$efficiency and measured σB[3, 4]. Figure 2 shows a plot of the measured σB for W and Z production at $\sqrt{s} = 630$ GeV[1, 2] and 1.8 TeV, compared with a QCD calculation.

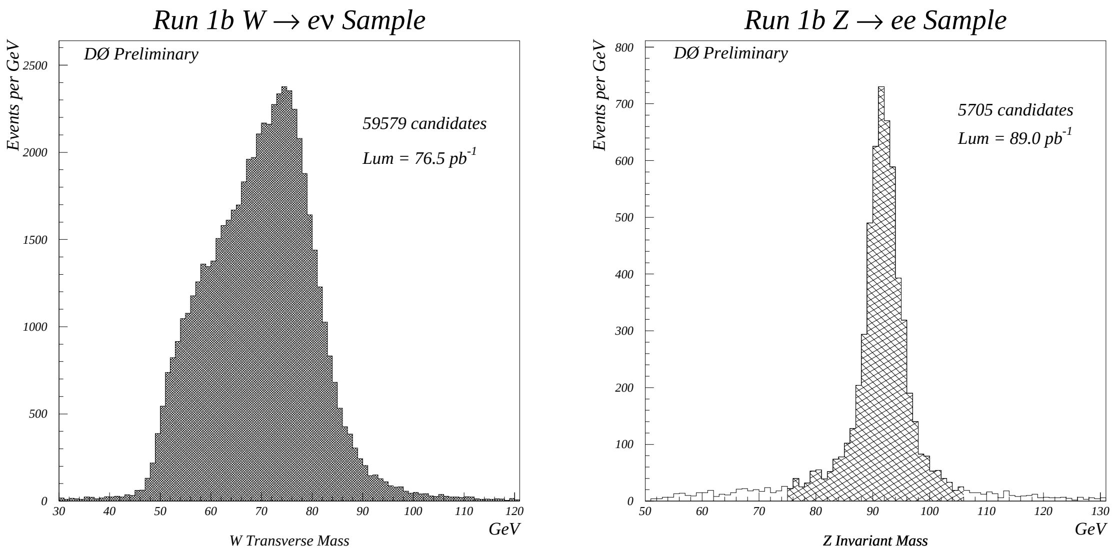

Figure 1: Transverse mass spectrum of DØ $W \rightarrow e\nu$ candidates from Run 1b (left) and invariant mass spectrum of DØ $Z \rightarrow ee$ candidates from Run 1b (right).

sample	quantity	$W \rightarrow e\nu$	$Z \rightarrow ee$	$W \rightarrow \mu\nu$	$Z \rightarrow \mu\mu$
DØ Run 1a	events	10338	775	1665	77
	background	590±50	31±11	370±30	8±3
	acc×eff	0.32±0.01	0.27±0.01	0.054±0.007	0.034±0.004
	σB (nb)	2.36±0.15	0.218±0.016	2.09±0.25	0.18±0.03
DØ Run 1b	events	≈60000	≈5700	≈7000	≈500
CDF Run 1a	events	13796	1312	6222	423
	background	1700±161	21±9	13.1±2.0	0.4±0.2
	acc×eff	0.26±0.01	0.30±0.01	0.12±0.01	
	σB (nb)	2.49±0.12	0.231±0.012	2.48±0.19	
CDF Run 1b	events	≈47000	≈5000	≈26000	≈2000

Table 2: Summary of cross section analyses.

3 W boson width measurement

The width of the W boson is predicted by the Standard Model to be 2.077±0.014 GeV [5]. If it decays into channels not predicted by the Standard Model then its width will deviate from the predicted value. At the Tevatron, there are two ways to measure this width.

The most precise method is to infer the W boson width from the observed ratio of W and Z production cross sections times leptonic branching fractions,

$$R = \frac{\sigma_W B(W \to \ell\nu)}{\sigma_Z B(Z \to \ell^+\ell^-)}. \tag{2}$$

In this ratio many systematic uncertainties approximately cancel, but theoretical input for σ_W/σ_Z and $,(W \to \ell\nu)$, and a measurement of $B(Z \to \ell^+\ell^-)$ are needed to extract the W boson width from

$$,_W = \frac{\sigma_W}{\sigma_Z}\frac{,(W \to \ell\nu)}{B(Z \to \ell^+\ell^-)R}. \tag{3}$$

The DØ measurement is $,_W = 2.044 \pm 0.093$ GeV [3] and the CDF measurement is $,_W = 2.063 \pm 0.086$ GeV [6]. Together with the measurements by UA1 [7] and UA2 [2] the best value for the W boson width is [3]

$$,_W = 2.062 \pm 0.059 \text{ GeV}, \tag{4}$$

in good agreement with the Standard Model prediction. These measurements limit the contribution of non-standard decays to the W boson width to 109 MeV at 95% confidence level.

The second method is a direct measurement of the width of the W boson from the tail of the transverse mass spectrum. CDF has performed this measurement with the sample of $W \to e\nu$ decays from Run 1a and measures $,_W = 2.11 \pm 0.32$ GeV [8]. This measurement is statistically less powerful, but does not rely on any theoretical input.

Figure 3 summarizes all measurements of the W boson width.

4 Lepton charge asymmetry in W decays

Charged leptons from the decay of W bosons produced in $p\bar{p}$ collisions exhibit a charge asymmetry with respect to the direction of the incoming proton beam, *i.e.*, the ratio

$$A(y) = \frac{N_+(y) - N_-(y)}{N_+(y) + N_-(y)}, \tag{5}$$

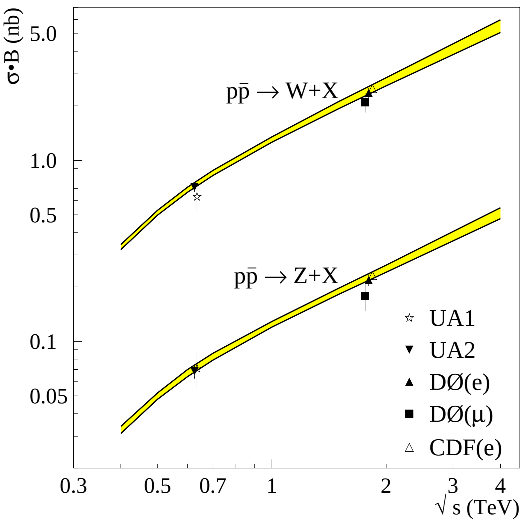

Figure 2: W and Z production cross section times leptonic branching fraction versus center of mass energy.

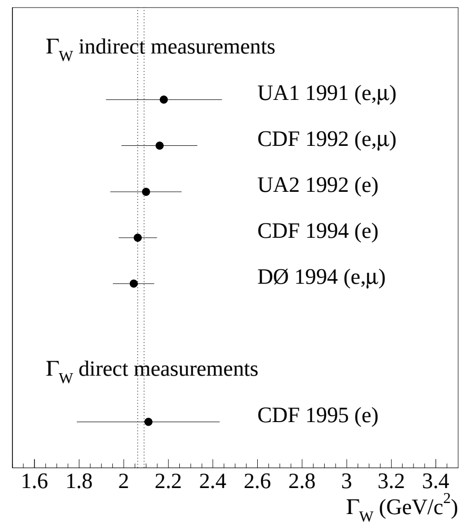

Figure 3: Comparison of all measurements of the W boson width.

where $N_{\pm}(y)$ is the number of leptons with charge ± 1 at rapidity y, varies with y. This asymmetry is due to two sources. W bosons are produced with an asymmetry, because u quarks carry a higher fraction of the proton momentum than d quarks. Since u quarks most of the time originate from the proton W^+ bosons produced in $u\overline{d}$ interactions more often move along the direction of the proton than the antiproton. The reverse is true for W^- bosons, which are produced in $\overline{u}d$ collisions. This production asymmetry is diluted by an asymmetry that arises from the $V-A$ coupling of the W boson to fermions. W bosons couple only to lefthanded fermions and righthanded antifermions. Since most often the quarks originate from the proton, the spin of W bosons points most of the time in the direction of the incoming antiproton beam and positively charged antileptons are emitted preferentially along the W boson spin, negatively charged leptons against the W boson spin direction.

Since the $V-A$ asymmetry is precisely predicted by the Standard Model, we can use a measurement of the lepton charge asymmetry to constrain the proton structure functions. Besides being interesting in its own right, this measurement also limits the uncertainty in the W mass measurement, described in the following section, due to uncertainties in our knowledge of the proton structure functions.

Figure 4 shows the magnitude of the observed lepton charge asymmetry $|A(y)|$ versus the magnitude of the lepton rapidity $|y|$. The data in the central region ($|y| < 1$) are from Run 1a[9] and 1b, in the forward region from Run 1a only, except the point at the highest rapidity, which is derived from $W \to \mu\nu$ decays detected in the forward muon system during Run 1b. The data points are compared to the prediction of some recent structure functions.

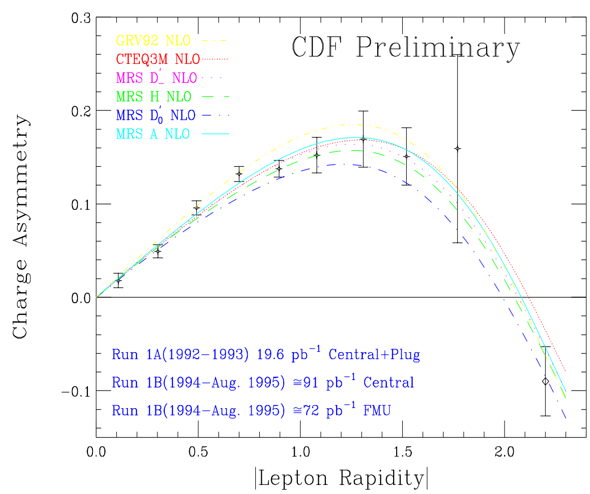

Figure 4: Lepton charge asymmetry measurement by CDF versus lepton rapidity.

5 W boson mass measurement

Given the mass of the Z boson, the Fermi constant, and the electromagnetic coupling constant at $Q^2 = m_Z^2$, the Standard Model predicts the mass of the W boson at tree level. Beyond tree level, fermion and boson loops (see figure 5) contribute to the mass, introducing sensitivities to other parameters of the Standard Model, in particular the masses of the top quark (m_t) and the Higgs boson (m_H). These corrections are proportional to m_t^2 (for $m_t \to \infty$) and $\ln m_H$ (for $m_H \to \infty$). A precise measurement of the W boson mass measures these radiative corrections and constrains the top and Higgs masses, and therefore provides a test of the Standard Model.

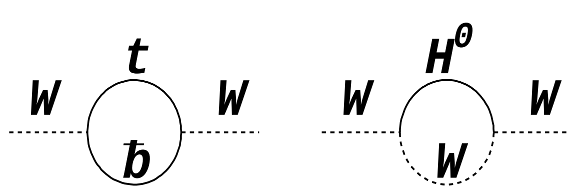

Figure 5: Loop diagrams contributing to the W boson mass.

DØ and CDF determine the W boson mass by fitting the transverse mass spectrum (equation 1). In order to predict the m_T spectrum as a function of the W mass a precise knowledge of the response and resolution of the detector to charged leptons and the particles recoiling against the W boson is required.

In the following I will describe the DØ W mass measurement in detail, since it is new, while the CDF measurement has been published already [10]. The most notable difference between the two measurements is that CDF calibrates the momentum measurement of the charged lepton against $J/\psi \to \mu^+\mu^-$ decays and DØ against $Z \to e^+e^-$ decays, thereby essentially measuring the W/Z mass ratio.

Beam tests of the DØ calorimeter have shown that its response to electrons has the form $E = \alpha p_{beam} + \delta$, where E is the measured electron energy and p_{beam} the known beam momentum. We determine the calibration constants α and δ from collider data by comparing the signal from three resonances that decay into electromagnetically showering particles, $\pi^0 \to \gamma\gamma$ (figure 6), $J/\psi \to e^+e^-$ (figure 7), and $Z \to e^+e^-$ (figure 9) to Monte Carlo predictions with different assumptions for the values of α and δ using a χ^2 test. The constraints obtained are shown in figure 8. The figure indicates the contours of $\chi^2 = \chi^2_{min} + 1$ for the three resonances separately and all three combined. Note that δ is determined primarily by the low mass resonances, while the scale is set by the Z data, once δ is known. The contours in the figure reflect statistical uncertainties only. The constraint on δ is in fact systematically limited by the uncertainty in the calorimeter response at low energies. We measure $\delta = -0.16^{+0.03}_{-0.21}$ GeV. An error in δ translates into an error in the measured W mass of 0.1 times the error in δ. For this value of δ we obtain $\alpha = 0.9514 \pm 0.0018$. We determine the electron energy resolution from the observed width of the $Z \to ee$ resonance. It can be parametrized as $\sigma/p = 0.015 \oplus 0.13/\sqrt{p_T} \oplus 0.4/p$ with all momenta in GeV.

Having calibrated electron response and resolution DØ uses the Z data to calibrate the response and resolution of the calorimeter to the recoil particles. Here the analysis exploits that one can reconstruct the Z completely from the two charged leptons and then compare the transverse momentum of the Z to that of the recoil. Both momenta are projected on the inner bisector of the two electron directions as shown in figure 10. The mean of the sum of the two projections is a measure of the recoil response and its rms width of the recoil resolution. The calorimeter response to the recoil particles is 0.83 ± 0.04 times the response to electrons. The sum of the two projections, corrected for the recoil response, is shown in figure 11.

A Monte Carlo simulation using the measured detector responses and resolutions pre-

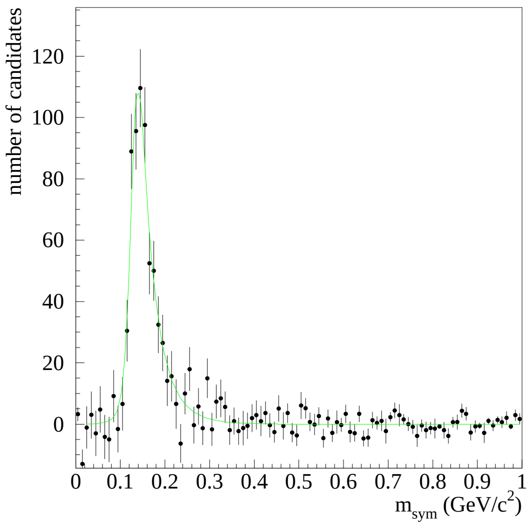

Figure 6: Observed $\pi^0 \to \gamma\gamma$ signal. The points show the background subtracted data and the smooth curve a Monte Carlo prediction of the line shape.

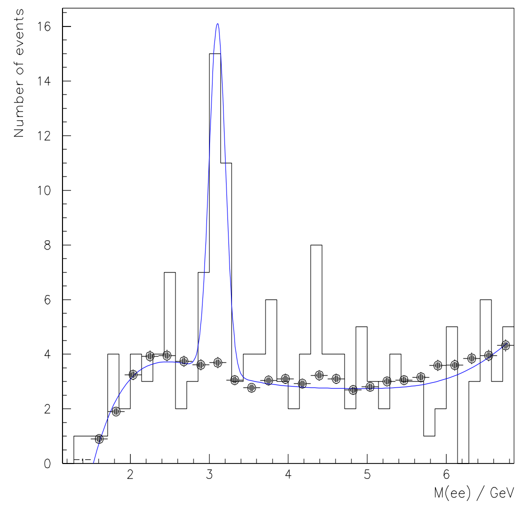

Figure 7: Observed $J/\psi \to e^+e^-$ signal. The histogram shows the data, the points the estimated background and the smooth curve a fit to the data.

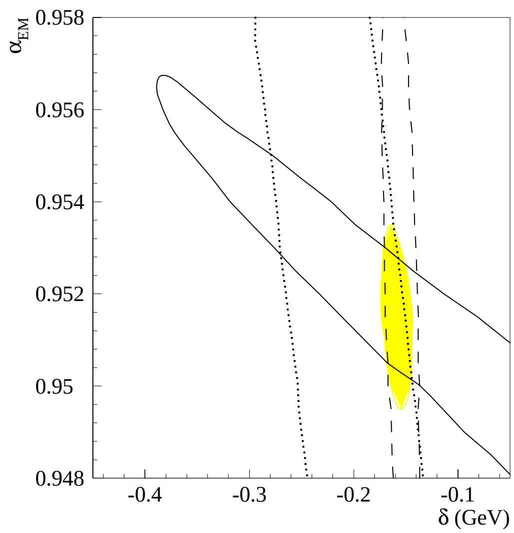

Figure 8: Contours of $\chi^2 = \chi^2_{min} + 1$ from π^0 data (- - -), J/ψ data (......), Z data (——) and combined (shaded).

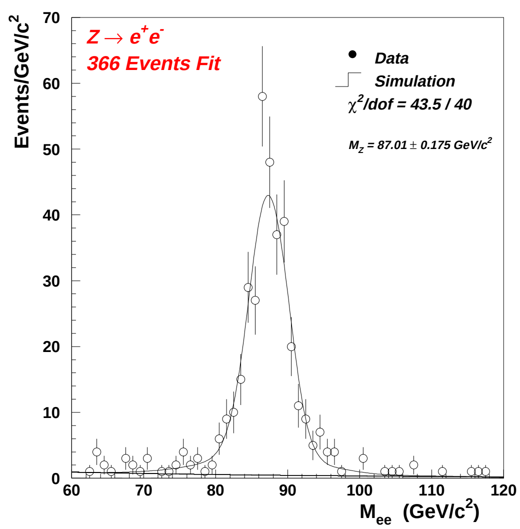

Figure 9: Observed $Z \to e^+e^-$ signal. The points show the data, the smooth curve is a Monte Carlo prediction.

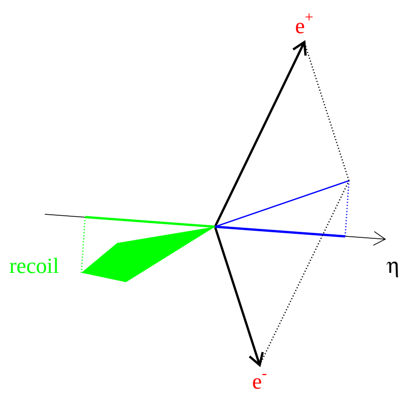

Figure 10: Definition of η-axis.

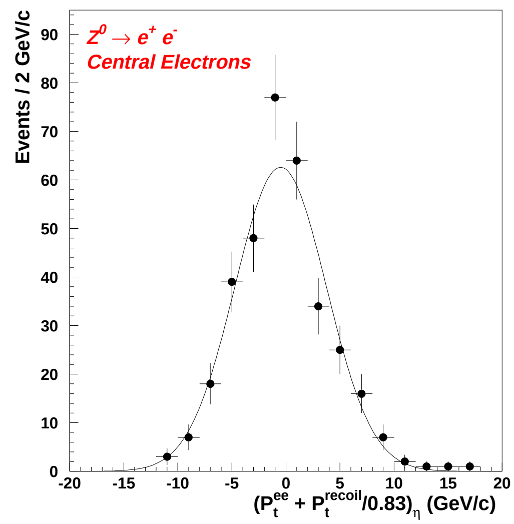

Figure 11: Spectrum of sum of projection of recoil p_T (corrected for response) and dielectron p_T onto η-axis.

dicts the shape of the m_T spectrum as a function of the W boson mass. The mass is determined using a maximum likelihood fit. Figure 12 shows the fit to the transverse mass spectrum. DØ determines the W boson mass in the $W \to e\nu$ channel to be $m_W = 80.35 \pm 0.14(\mathrm{stat}) \pm 0.23(\mathrm{syst})$ GeV. The CDF measurement for the $W \to e\nu$ and $W \to \mu\nu$ channels combined is $m_W = 80.41 \pm 0.18$ GeV. Table 3 lists the systematic uncertainties in detail. Combining these results with the earlier CDF [11] and UA2 [12] results yields a world average of

$$m_W = 80.34 \pm 0.15 \text{ GeV}, \tag{6}$$

in good agreement with the result of a global fit to the LEP and SLC data [13], which predicts $80.36 \pm 0.05^{+0.013}_{-0.024}$ GeV, where the second error quantifies the variation of this value with the Higgs mass. Figure 13 shows a plot of the correlation between W boson and top quark masses introduced through the loop diagrams shown in figure 5. The shaded bands show the region allowed by the Standard Model for different Higgs masses. The DØ and CDF W and top mass [14] measurements are shown. They are in good agreement with the Standard Model, but not yet precise enough to constrain the mass of the Higgs boson.

source	uncertainty in MeV		
	DØ (e)	CDF (e)	CDF (μ)
statistical	140	145	205
systematics	225	175	130
lepton response	160	120	50
lepton resolution	70	80	60
angle calibration	50	—	—
recoil modeling	105	65	60
backgrounds	35	10	25
selection biases	30	—	25
W production, decay	70	75	75

Table 3: Sources of uncertainty in the W mass measurement.

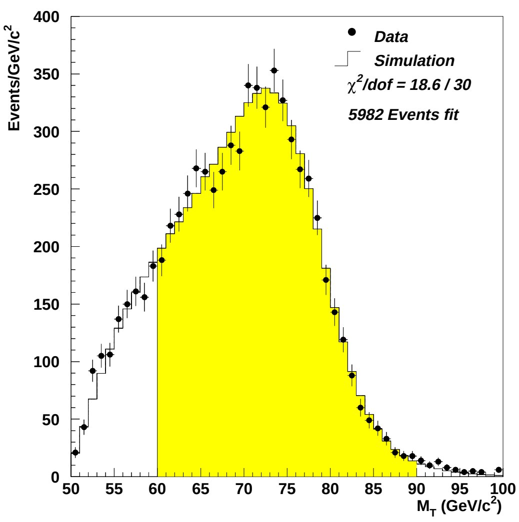

Figure 12: Fit to transverse mass spectrum observed by DØ. The histogram shows the Monte Carlo prediction for the fitted mass.

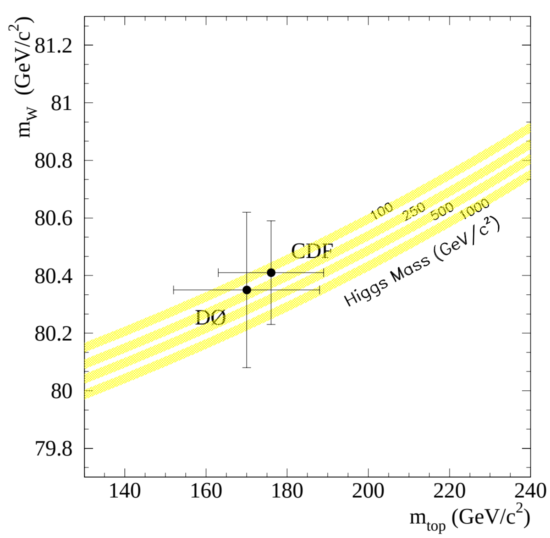

Figure 13: Correlation of W and top masses in the Standard Model and the DØ and CDF measurements.

6 Trilinear gauge boson couplings

The Standard Model predicts the existence of $WW\gamma$ and WWZ triple gauge boson couplings. These vertices can in general be described by an effective Lagrangian with four independent couplings [15], denoted by κ_V, λ_V, $\tilde{\kappa}_V$, and $\tilde{\lambda}_V$ $(V = Z, \gamma)$. The former two describe the strength of CP conserving and the latter two of CP violating amplitudes. In the Standard Model

$$\kappa_V = 1, \quad \lambda_V = \tilde{\kappa}_V = \tilde{\lambda}_V = 0. \tag{7}$$

Tree level unitarity constrains all couplings to their Standard Model values at high energies. It is therefore customary to introduce form factors $\left(1 + \frac{s}{\Lambda^2}\right)^{-n}$, where Λ is the form factor scale. For the WWV vertices a dipole form factor is used $(n = 2)$. We can study these triple gauge boson couplings via diboson ($W\gamma$, WW, WZ) production. Non-standard couplings would manifest themselves in an increased cross section and a harder p_T spectrum of the bosons.

The following diagrams contribute to $W\gamma$ production.

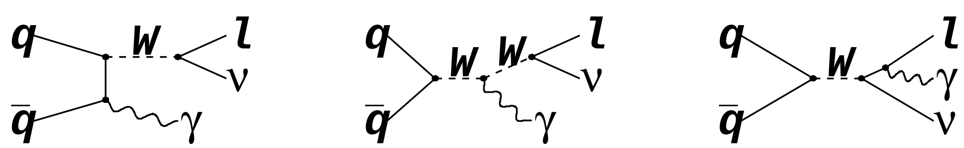

$W\gamma$ events are selected by tagging the W decays via a high p_T electron or muon and missing p_T due to the neutrino. The photon is required to have at least 10 GeV (7 GeV) p_T for the DØ (CDF) analysis and must be well separated from the charged lepton ($\sqrt{\Delta\eta^2 + \Delta\phi^2} > 0.7$) to suppress final state radiation. Table 4 summarizes the event yields of both experiments. The number of events observed is consistent with Standard Model expectations plus background.

	DØ 1a [16] 14 pb^{-1}	DØ 1b 55 pb^{-1}	CDF 1a[17]+1b 67 pb^{-1}
events	23	36	109
background	6.4±1.4	8.4±1.7	26.4±3.1
Standard Model	13.5	32.5	75.3

Table 4: Summary of $W\gamma$ event yields.

The most powerful limits on the couplings can be obtained from fits to the shape of the photon p_T spectra, which are shown in figures 14 and 15. Figure 16 shows the preliminary 95% confidence level contours in the κ_γ-λ_γ plane, assuming $\widetilde{\kappa}_\gamma = \widetilde{\lambda}_\gamma = 0$. The 95% confidence level limits on κ_γ and λ_γ, assuming the other three couplings have their Standard Model values and $\Lambda = 1.5$ TeV, are (see [16, 17] for Run 1a results).

$$\begin{array}{lrclrcl} \text{DØ (1a+1b)} & -1.42 & < \kappa_\gamma - 1 < & 1.39 & -0.41 & < \lambda_\gamma < & 0.40 \\ \text{CDF (1a+1b)} & -1.8 & < \kappa_\gamma - 1 < & 2.0 & -0.7 & < \lambda_\gamma < & 0.6 \end{array} . \tag{8}$$

Standard Model $WW \to \ell\nu q\bar{q}$ and $WZ \to \ell\nu q\bar{q}$ production is swamped by W+jets production. However there is sensitivity to non-standard couplings at high boson p_T. The 95% confidence level limits obtained assuming $\kappa_\gamma{=}\kappa_Z{=}\kappa$, $\lambda_\gamma{=}\lambda_Z{=}\lambda$ and $\Lambda = 1.5$ TeV are

$$\begin{array}{lrclrcl} \text{DØ (1a)} & -0.9 & < \kappa - 1 < & 1.1 & -0.7 & < \lambda < & 0.7 \\ \text{CDF (1a+1b)} & -0.67 & < \kappa - 1 < & 0.85 & -0.51 & < \lambda < & 0.50 \end{array} . \tag{9}$$

In the channel $WW \to \ell\nu\ell'\nu'$ DØ set an upper limit of 87 pb on the production cross section using data from Run 1a only, which implies [18]

$$\text{DØ (1a)} \quad -2.6 < \kappa - 1 < 2.8 \quad -2.1 < \lambda < 2.1 \tag{10}$$

with $\Lambda = 0.9$ TeV. CDF has measured the cross section using their data from Run 1a and part of 1b (67 pb^{-1}) to be $13.8^{+9.6}_{-7.9}$ pb, compared to a Standard Model prediction of 9.5 pb.

DØ has combined the limits from $W\gamma$, WW and WZ production from the Run 1a data and obtains

$$\text{DØ (1a)} \quad -0.71 < \kappa - 1 < 0.89 \quad -0.44 < \lambda < 0.44 \; . \tag{11}$$

$ZZ\gamma$ and $Z\gamma\gamma$ interactions can also be described by four amplitudes with coupling constants h_1, h_2, h_3, h_4. In the Standard Model these vertices do not exist and

$$h_1 = h_2 = h_3 = h_4 = 0. \tag{12}$$

These couplings can be studied via $Z\gamma$ production, in analogy to the $W\gamma$ analysis. Again the most stringent limits on the couplings are obtained from fits to the photon p_T spectra, which are shown in figures 17 and 18. Figure 19 shows the 95% confidence level contours in the h_4-h_3 plane assuming that all other couplings vanish. Assuming the other three couplings vanish and $\Lambda = 0.5$ TeV the limits are (see [19, 20] for Run 1a results)

$$\begin{array}{lrclrcl} \text{DØ (1a)} & -1.8 & < h_3 < & 1.8 & -0.5 & < h_4 < & 0.5 \\ \text{CDF (1a+1b)} & -1.6 & < h_3 < & 1.6 & -0.4 & < h_4 < & 0.4 \end{array} . \tag{13}$$

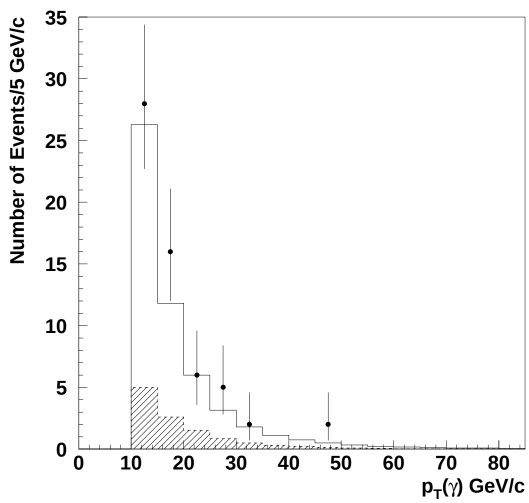

Figure 14: Photon p_T spectrum from the DØ $W\gamma$ data (1a and partial 1b). The histograms show the expected signal plus background and the background.

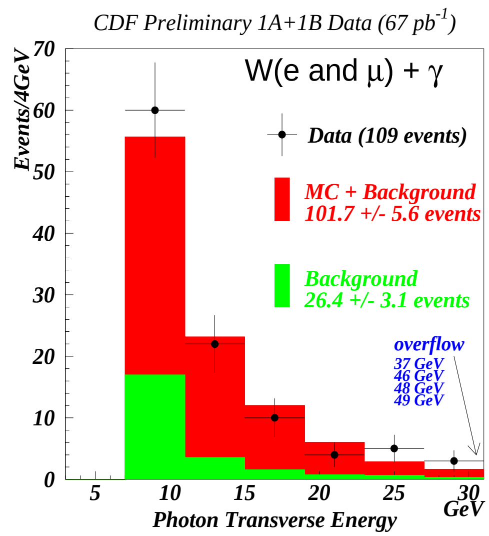

Figure 15: Photon p_T spectrum from the CDF $W\gamma$ data (1a and partial 1b). The histograms show the expected signal plus background and the background.

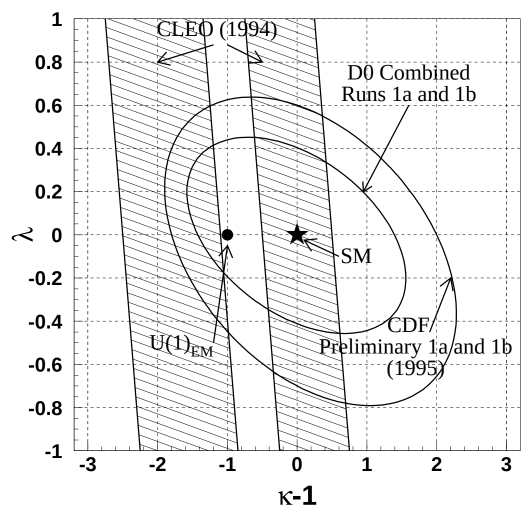

Figure 16: 95% confidence level contours in the κ_γ-λ_γ plane, assuming $\tilde{\kappa}_\gamma = \tilde{\lambda}_\gamma = 0$.

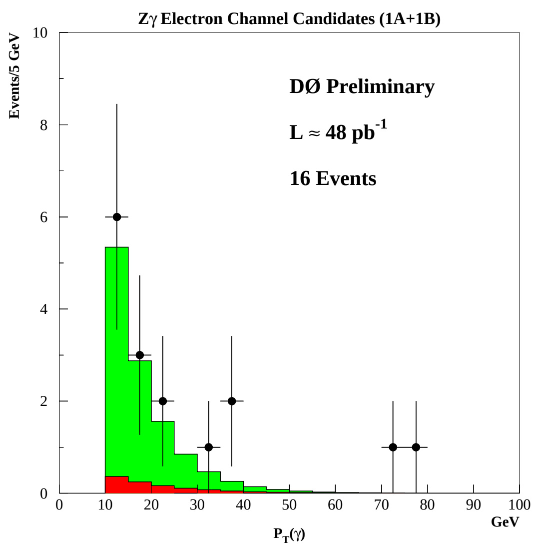

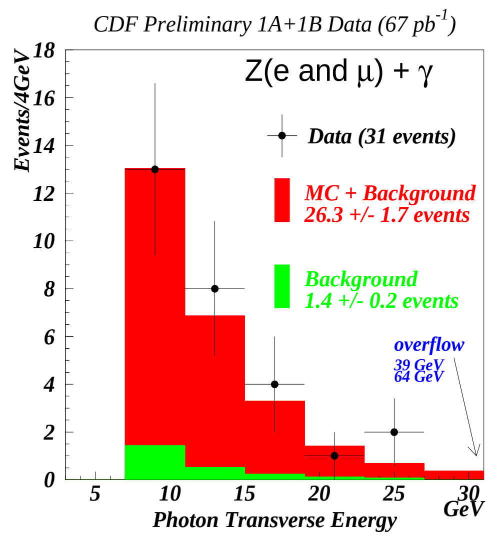

Figure 17: Photon p_T spectrum from the DØ $Z\gamma$ data (1a and partial 1b). The histograms show the expected signal plus background and the background.

Figure 18: Photon p_T spectrum from the CDF $Z\gamma$ data (1a and partial 1b). The histograms show the expected signal plus background and the background.

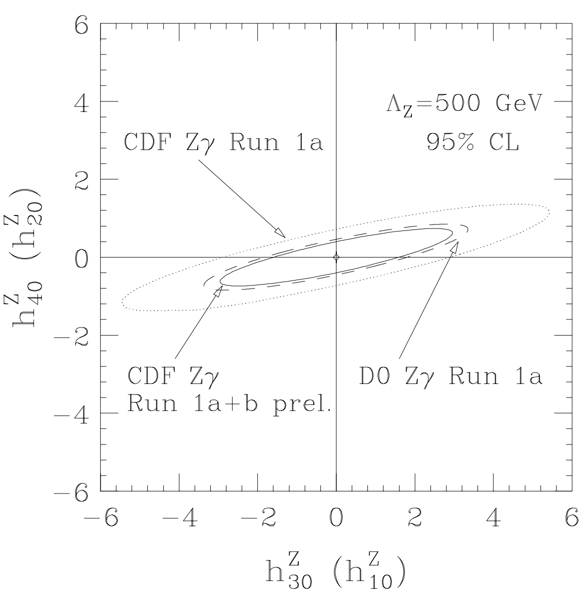

Figure 19: 95% confidence level contours in the h_4-h_3 plane.

7 Conclusions

Both experiments at the Tevatron have accumulated data sets of about 100 pb^{-1}. Using partial data sets the DØ and CDF experiments have measured the mass and width of the W boson. Both experiments have observed diboson production and measured the triple gauge boson couplings. No deviations from Standard Model predictions have been observed. A substantial increase in precision is expected from the analysis of the full data sets, which is presently under way.

I should like to thank the organizers for a very interesting and stimulating meeting and my CDF and DØ colleagues for their help in preparing this presentation.

References

[1] Albajar *et al.* (UA1), Z. Phys. C **44**, 15 (1989).

[2] Alitti *et al.* (UA2), Phys. Lett. B **276**, 365 (1992).

[3] Abachi *et al.* (DØ), Phys. Rev. Lett. **75**, 1456 (1995).

[4] Abe *et al.* (CDF), Phys. Rev. Lett. **76**, 3070 (1996).

[5] Rosner, Worah, Takeuchi, Phys. Rev. D **49**, 1363 (1994).

[6] Abe *et al.* (CDF), Phys. Rev. Lett. **73**, 220 (1994); Phys. Rev. D **52**, 2624 (1995).

[7] Albajar *et al.* (UA1), Phys. Lett. B **253**, 503 (1991).

[8] Abe *et al.* (CDF), Phys. Rev. Lett. **74**, 341 (1995).

[9] Abe *et al.* (CDF), Phys. Rev. Lett. **74**, 850 (1995).

[10] Abe *et al.* (CDF), Phys. Rev. Lett. **75**, 11 (1995); Phys. Rev. D **52**, 4784 (1995).

[11] Abe *et al.* (CDF), Phys. Rev. Lett. **65**, 2243 (1990).

[12] Alitti *et al.* (UA2), Phys. Lett. B **276**, 354 (1992).

[13] Renton, Oxford University Preprint OUNP-95-20.

[14] Abe *et al.* (CDF), Phys. Rev. Lett. **74**, 2626 (1995); Narain (DØ), these proceedings.

[15] Baur, Berger, Phys. Rev. D **41**, 1476 (1990).

[16] Abachi *et al.* (DØ), Phys. Rev. Lett. **75**, 1034 (1995).

[17] Abe *et al.* (CDF), Phys. Rev. Lett. **74**, 1936 (1995).

[18] Abachi *et al.* (DØ), Phys. Rev. Lett. **75**, 1023 (1995).

[19] Abachi *et al.* (DØ), Phys. Rev. Lett. **75**, 1028 (1995).

[20] Abe *et al.* (CDF), Phys. Rev. Lett. **74**, 1941 (1995).